DOI : 10.1002/(ISSN)1545-2263
ISSN (print) : 1545-2255
ISSN (electronic) : 1545-2263
ID (product) : STC
Title (main) : Structural Control and Health Monitoring
Title (short) : Struct Control Health Monit
DOI : 10.1002/stc.v9999.9999

Numbering (journalVolume) : 9999
Numbering (journalIssue) : 9999
CoverDate : 2020
DOI : 10.1002/stc.2517
ID (unit) : STC2517
ID (society) : STC-18-0262.R2
ID (eLocator) : e2517
Count (pageTotal) : 1
Title (articleCategory) : RESEARCH ARTICLE
Title (tocHeading1) : RESEARCH ARTICLES

Event (manuscriptReceived) : 2018-07-26
Event (manuscriptRevised) : 2019-11-19
Event (manuscriptAccepted) : 2020-01-08
Event (xmlCreated) : 2020-01-18 (SPi Global)
Numbering (pageFirst) : n/a
Numbering (pageLast) : n/a

SelfCitationGroup : Andreaus U, De Angelis M. Influence of the characteristics of isolation and mitigation devices on the response of single-degree-of-freedom vibro-impact systems with two-sided bumpers and gaps via shaking table tests. *Struct Control Health Monit*. 2020;e2517. https://doi.org/10.1002/stc.2517

Object Name (appendix) : APPENDIX
Link (toTypesetVersion) : file:stc2517.pdf
Link (toAuthorManuscriptVersion) : file:stc2517_am.pdf

Short Authors: Andreaus and De Angelis

Influence of the characteristics of isolation and mitigation devices on the response of single-degree-of-freedom vibro-impact systems with two-sided bumpers and gaps via shaking table tests<<Query: AUTHOR: Per journal instruction,

abbreviations are not allowed in the article title; hence, “SDOF” has been defined. Please confirm this is correct.>>

Ugo<<Query: AUTHOR: Please verify that the linked ORCID identifiers are correct for each author.>><<Query: AUTHOR: Please confirm that forenames/given names (blue) and surnames/family names (vermilion) have been identified correctly.>> Andreaus*[1], Maurizio De Angelis[1]

[1] Dipartimento di Ingegneria strutturale e geotecnica, Sapienza Università di Roma, Roma, Italy

Ugo Andreaus: ✉ ugo.andreaus@uniroma1.it

*Correspondence to:

<<Query: AUTHOR: Please confirm that authors' affiliation and correspondence details are correct.>>Correspondence

Ugo Andreaus, Dipartimento di Ingegneria strutturale e geotecnica, Sapienza Università di Roma, Via Eudossiana 18-00184 Roma, Italy.

Email: ugo.andreaus@uniroma1.it

FundRef Name	FundRef Organization Name	Funding Number
<<Query: AUTHOR: “Italian Ministry of University and Research” was identified as funder in the supplied metadata, however, this funder was not mentioned in the acknowledgments or funding information section. Please insert the appropriate text for this funder, or confirm that this is to be deleted from the funders list.>>Italian Ministry of University and Research		2010MBJK5B-005

Summary

During strong earthquakes, structural pounding may occur between structures (buildings, bridges, strategic facilities, critical equipment, etc.) and the surrounding moat wall because of the limited separation distance and the deformations of the isolator. An arrangement that favors the solution of this problem is the interposition of shock absorbers. Thus, the influence of geometrical and mechanical characteristics of isolation and mitigation devices on nonlinear, nonsmooth response of vibro-impact systems is experimentally investigated in this paper on the basis of a laboratory campaign of experimental tests. Shaking table tests were carried out under a harmonic excitation in order to investigate two different configurations: the absence and the presence of bumpers. Three different values of the table acceleration peak were applied, four different amplitude values of the total gap between mass and bumpers were considered, and also four different types of bumpers were employed; moreover, two problems were addressed, namely, control of excessive displacements and control of excessive accelerations, and hence, two types of normalization were adopted in order to better interpret experimental results. Suitable choices of pairs of bumpers and gaps were suggested as a trade-off between conflicting objectives. Furthermore, a numerical model was proposed, and its governing parameters identified in order to simulate the experimental results.

Keywords: displacement and acceleration control; seismic protection; shaking table; structural pounding; two-sided bumpers; vibro-impact system

1 INTRODUCTION

In earthquake<<Query: AUTHOR: Please check the hierarchy of the section headings if presented correctly.>>-prone areas, civil structures experience exceptional loading conditions that may result in wide undesirable losses and damage. Seismic isolation systems are essentially designed to preserve structural safety and prevent occupants' injury and properties' damage. The major concept in base isolation is to diminish the fundamental frequency of structural vibration to a value lower than the dominant energy frequencies of earthquake ground motions.[1, 2]

However, seismically isolated structures are expected to experience large displacements relative to the ground especially under near-fault (NF) earthquakes. The NF ground motions are characterized by one or more intense long-period velocity and displacement pulses, which lead the isolator to undergo large displacements[2–4] and—possibly—to be seriously damaged by exceeding the limit deformation and hence remaining permanently deformed or rupture can even occur. Such large displacements are accommodated by providing a sufficient seismic gap around the isolated structure. In some cases, the width of the provided seismic gap is limited because of practical constraints.[2]

Base isolation is used on different scales, from decoupling a superstructure from its substructure[5] resting on a shaking ground, thus protecting a building or nonbuilding structure's integrity down to a single room in a building. Floor isolation technology can be an efficient and cost-effective means for providing seismic protection for precision equipment or delicate works of art.[6–8]

1.1 Damages because of large displacements in based isolated systems

Because of the greater flexibility offered by the isolators at the base, seismically isolated buildings can exhibit large relative horizontal displacements during strong seismic excitations, just in the case they contain long-period pulses, which characterize NF earthquakes. Therefore, in the event of a strong earthquake, it should be taken into account that the seismically isolated structure can face the risk of the occurrence of colliding with a surrounding retaining wall or other adjacent constructions.[9]

The performance of structures with respect to earthquake excitation can be improved by the technique of seismic isolation, which has often proved to be an effective tool for earthquake-resistant design. Although floor isolation reduces the risk of damage to a building, because of greater flexibility, it causes a significant drift at the level of isolation. In order to account for large relatively displacements, it is necessary to provide a large seismic clearance as free space around the building. A practical limitation is imposed by this specification on the use of earthquake isolation, because there are often limitations in the amount of clearance available in the presence of seismically isolated buildings, which will later be referred to as gaps, particularly in the practice of adaptation and reinforcement of existing constructions, situated in metropolitan zones. Thus, the danger of impact on the surrounding moat walls or adjacent structures during severe earthquakes and the likely consequences of these undesired events are of great importance.[10]

1.2 Damages because of large accelerations in based isolated systems and equipment

The results from numerical simulations and parametric studies that have been conducted in the papers of Komodromos et al.[11] and Polycarpou and Komodromos[9] demonstrated the detrimental effects of potential poundings on the effectiveness of seismic isolation. In particular, both floor accelerations and interstory deflections of a seismically isolated building increase because of impact, either with the surrounding moat

wall or with adjacent buildings. Both accelerations at floor levels and displacements between stories are importantly magnified when structural pounding occurs, menacing the vulnerable equipment roomed in the structure and the operation of the structure itself.[11–14] In more detail, the acceleration response exhibits impulses characterized by large frequency and amplitude, the latter being influenced by impact rigidity, in correspondence of the floors where pounding occurs. Therefore, pounding can cause a very crucial problem that is represented by the existence of high spikes in the acceleration response; this problem is particularly accentuated in the case of vulnerable equipment hosted in the buildings.[15] Moreover, in the case of industrial and power generation facilities, acceleration spikes may influence floor response spectra and thus the response of equipment.[16] Thus, considering practical interventions finalized to obtain the mitigation of the impact effects seems to be a very notable task.[17]

1.3 Classification

A first aim of this work is precisely that of framing the problem of pounding in its various aspects. For simplicity's sake, the considered structural configurations can be schematically grouped into the following types:

- Pounding of ADJacent structures (PADJS)
  - Buildings
  - Bridges
- Pounding of base-isolated structures (PBIS)
  - Building
  - Equipment

Three situations are considered: pounding (a) between adjacent structures, (b) of base-isolated building against retaining walls, and (c) of base-isolated building against retaining walls and adjacent structures.

1.4 PADJS—Buildings

1.4.1 Connection by dampers

The probability that during strong earthquakes, pounding of seismically isolated structures with the neighboring adjacent structures (PADJS) occurs may represent an inescapable problem. In this respect, the case of common buildings has been the object of important studies,[18–23] which considered adjacent buildings connected by shock absorbers.

The papers[18–20, 23] present theoretical procedures for mitigating earthquake-induced pounding of adjacent buildings linked by dampers. Two adjacent structures are connected by linear visco-fluid

dampers,[18, 19] by linear visco-elastic[23, 24] and visco-fluid damper,[23] and by friction damper under harmonic ground acceleration.[20] Each structure is modeled as a single-degree-of-freedom (SDOF) system[19, 20] and as 2-D and 3-D multi-degree-of freedom (MDOF) systems, respectively.[18, 23] Zhang and Xu[18] and Zhu et al.[23] use a numerical approach, whereas Zhu and Xu[19] give analytical formulas and Bhaskararao and Jangid[20] give closed-form solutions for determining seismic response of adjacent buildings linked by dampers. In Agarwal et al.,[24] the earthquake-induced pounding in friction varying base-isolated buildings is investigated.

1.4.2 Impact by bumpers

The mitigation of pounding induced by earthquake between steel structures through the interposition of shock absorbers between the colliding members are the focus of the papers.[15, 16, 25–30] The constitutive relations between impacting systems can be modeled in different ways. A summary subdivision can be made in two general groups: hard and soft impacts. The former is based on the concept of restitution coefficient,[24–26] where the contact time is assumed to be infinitely small and the deformation in the contact zone to be negligible, whereas the latter presumes contact time of finite duration, and a penetration between colliding bodies is admitted. Therefore, linear,[29] Hertzian,[31, 32] or alternative nonlinear springs and viscous dampers[15, 16, 27, 28, 30] are used to model the contact.

The effectiveness of using dissipative and deformable bumpers to mitigate potential earthquake-induced pounding was investigated numerically by Polycarpou et al.[15] and experimentally by Chase et al.,[25] utilizing 2-D MDOF structural models.

Wang et al.,[26] Mate et al.,[28] Bamer et al.,[29] Wang et al.,[30] and Crozet et al.[16] presented numerical studies devoted to the analysis of building pounding for SDOF[16, 26, 30] and MDOF[28, 29] (Bamer et al.[29] in 2-D and Mate et al.[28] in 3-D) systems, under seismic[16, 28, 29] and impulsive excitation.[26, 30]

1.5 PADAJS—Bridges

Bridges can be particularly sensitive to pounding because it can cause the failure of the decks because of local damage involving crushing and spalling of girders and of supports between girders and piers and of limiters between adjacent girders. A survey about impact models, results of experimental researches, and techniques devoted to mitigate the effects of pounding induced by earthquake excitation between bridge decks can be found in Hao et al.,[33] whereas further results of both experimental and analytical investigations concerning pounding of isolated bridges are reported in other works.[34, 35]

Bridges have also been separately analyzed in many cases.[34, 36–40] Furthermore, a wide literature[34, 40–42] published the results obtained by conducting pounding experiments on framed buildings and highway bridges. In particular, pounding response of bridge superstructures subjected to ground motions varying in space has been studied by Li-Xiang et al.[43] in both experimental and analytical way.

1.6 PBIS—Moat wall

In the context of earthquake-induced pounding of PBIS, Tsai[44] investigated the effects of pounding on structural response by simulating the superstructure of an isolated building as a continuous shear beam and observing a very high acceleration response during pounding with the surrounding moat wall in correspondence of the isolation level. Similar work was done by Malhotra,[31] who found that the increase of stiffness of isolated structure or of surrounding moat wall induces the increase of base shear forces. The damaging effects of structural impact on the effectiveness of seismic isolation were revealed by the parametric analysis conducted by Komodromos et al.[11] on pounding of a seismically isolated building with the surrounding moat wall.[11, 45]

The main objective of the applicative[10, 11, 14, 17, 46] and theoretical[47] studies is to examine through numerical simulations[10, 11, 17, 46, 47] and also experimentally evaluate[14, 47] the effects of structural pounding at the base-isolated level in building structures—which are subjected to strong earthquakes—and the resulting dynamic response of the superstructure.

Base pounding theoretical models with linear spring-gap element are proposed in Mavronicola et al.[10] and Liu et al.,[46] whereas Komodromos et al.,[11] Polycarpou and Komodromos,[17] Masroor and Mosqueda,[14, 47] Mavronicola et al.,[10] and Liu et al.[46] formulate nonlinear impact elements that can simulate the contact force during impact of base-isolated structure to a moat wall; the moat wall was modeled as either a concrete wall with soil backfill or a rigid steel plate[14, 47] and as two-sided rubber bumpers.[10, 11, 17, 46]

The results for two-dimensional MDOF models are discussed in Komodromos et al.,[11] Polycarpou and Komodromos,[17] Masroor and Mosqueda,[14, 47] and Mavronicola et al.,[10] whereas three-dimensional finite element analyses are conducted by Liu et al.[46]

1.7 PBIS and PADJS

Section 1.6 contemplates the occurrence of impact of the building against the retaining moat wall exclusively in correspondence of the level where the isolator is located, in each case when the displacement of the building base exceeds the clearance of the gap (PBIS), during severe earthquakes. The other situations where other buildings are adjacent to the seismically isolated building under consideration and the drift of their superstructures is significant encounter the risk of poundings also in correspondence of the upper floors, as well as at ground level (PBIS and PADJS).

Matsagar and Jangid[32] studied the effects of using different base isolation techniques on the seismic response of multistory buildings, when is foreseen the possibility of collision against contiguous structures. In more detail, a relation of accelerations of upper floors in terms of isolation gap and the existence of a gap threshold was noticed, according which an increasing trend up to the threshold and then a decreasing trend were observed. Furthermore, the greater the flexibility of superstructures, the number of stories, and the stiffness of adjacent buildings, the more serious the consequences of pounding. The paper of Polycarpou and Komodromos[48] studied the pounding of an isolated building with adjacent structures both at the base level and at upper floors (PBIS and PADJS) and demonstrated that the collision of the building under examination with neighboring constructions cannot be excluded even in the case a sufficiently wide clearance is allowed for preventing impact against the retaining moat wall, because of excessive floor drifts.

In these applicative papers, the impact response of base-isolated multistory (MDOF in 2-D) buildings is numerically investigated under different real earthquake ground motions.

In particular, one of the specific objectives of Matsagar and Jangid[32] is to study the performance of different nonlinear and friction-based isolation systems during impact, whereas Polycarpou and Komodromos[48] simulate the behavior of the seismic isolation system by using a bilinear inelastic model.

In these studies, a force-based impact model is used, assuming an impact spring and an impact dashpot exerting, in parallel, impact forces to the colliding structures whenever their separation distances are exceeded (linear viscoelastic impact model).

Pant and Wijeyewickrema[49] studied the seismic pounding of a 4-story building in reinforced concrete isolated at the base. They considered three configurations characterized by (a) one moat wall on one the right side, (b) a similar building fixed at the base on the right side, and (c) two moat walls on both sides. Material and geometrical nonlinearities are accounted for by carrying out 3-D finite element analyses, in order to evaluate the structural performances of base-isolated buildings subjected to different seismic excitations.

1.8 Inner and outer pounding

Devices that enable the continuous activity of computing facilities, transmission networks, and life saver systems reduce the risk of material, economic, and human damages by moderating earthquake hazards. A promising answer for ensuring mission-critical systems and valuable assets from earthquake threats is represented by equipment isolation. Different isolation techniques have been proposed, developed, and employed in structures and equipment, such as friction pendula, rolling and sliding isolators, and bearings. The principle of operation is basically the same: The horizontal components of the ground (or floor) movement are mechanically separated from the isolated structure (or equipment) through compatible, sliding, rotating, or rolling interfaces.[50] In rolling isolation systems proposed by Harvey and Gavin,[50] Harvey et al.,[51] and Harvey and Gavin,[52] the limited rolling of steel spheres encapsulated between convex surfaces is employed in order to confine the displacement of the ball by means of a lip located at the border of every rolling surface. The roll-n-cage isolators[2, 53, 54] limit the peak isolator displacements and prevent PADJS under strong seismic excitation by using a self-braking mechanism, which contains the pounding inside the roll-n-cage isolator's frame. In friction pendulum isolators,[7, 55] if large displacements are attained, the slider element continues its motion on only one of the concave surfaces, when possible impact against the limiting ring prevents it to slide any longer on the other concave surface. Furthermore, also the high damping rubber bearing devices are inside self-braking seismic isolators (by constitutive law), with possible out pounding. In fact, experimental results[56, 57] revealed that the high damping rubber bearing exhibits strong nonlinearities and stiffening behaviours when large shear strains are attained because of a strain crystallization process in the rubber.[58]

The problem of outer pounding has been dealt with in the subsections “Impact by bumpers,” “PADJS—Bridges,” “PBIS—Moat wall,” and “PBIS and PADJS” and therefore we will not return to the topic in this subsection.

1.9 Authors' state of the art and aim of the paper

The problem of the impact of structures against moat walls and in particular of the base-isolated structures inspired the theoretical-numerical work presented in Andreaus and De Angelis.[59]

In order to simulate the response of these structures, a sufficiently general SDOF oscillator model was proposed consisting of a mass isolated by means of an isolator and impacting on two symmetrically spaced bumpers on the sides. A numerical investigation was carried out on the basis of this model, enabling the authors to outline possible scenarios within the system response. This purely numerical investigation was also carried out in order to guide the subsequent experimental activities. The results of preliminary experimental studies were presented in Andreaus et al.[60, 61] In particular, the first paper[60] was used to check the operation of the experimental equipment and verify the feasibility of the designed experiments, using one type of bumper, one gap width and four values of the table acceleration; whereas the second paper[61] was designed to individually characterize the mechanical behavior of the damper and bumpers prior to the shake table tests also in relation to the strain rate and to verify the potential differences in the dynamic response of the system with respect to different bumpers, gaps, and accelerations of the table; for this purpose, two types of bumpers, two amplitudes of gaps for each type of bumper, and at most four accelerations of the table in the case of a bumper and a gap were used. This prior activity has had the character of exploration.

As can be seen from the previous survey of the scientific literature on this subject, there are not many papers simultaneously dealing with the problems of (a) determining the effects of pounding in terms of damages, (b) mitigating pounding itself in the case of base-isolated structures from both a theoretical and experimental point of view, and (c) analyzing the influence of the most important parameters on the system response, such as gaps, mechanical parameters bumpers, input (intensity of harmonic excitation).

In this regard, the present work aims to present and comment the results obtained by carrying out a campaign of experimental investigations that is relatively extensive, limited to the table's performances and to the characteristics of the experimental setup, as illustrated in Section 2, by using a shaking table. In particular, the experimental setup has been improved by replacing the spherical bearings to the wheels, reducing the

friction phenomena and the risk of misalignment. See Tables 1 and 2 and Figure 1 for a more precise survey and comparison.

Table 1 Investigated cases

	a_G		0.03	0.04	0.05	0.075	0.1
NB	B0		x	x	x	—	—
YB	B1	G1	x	x	x	—	—
		G2	x	x	x	—	—
		G3	x	x	x	—	—
		G4	x	x	x	—	—
	B2	G1	x	x	x	—	—
		G2	x	x	x	—	—
		G3	x	x	x	—	—
		G4	x	x	x	—	—
	B3	G1	x°	x	x°	—	—
		G2	x	x	x	—	—
		G3	x	x	x°	x⁺	—
		G4	x	x	x	—	—
	B4	G1	x	x	x	—	—
		G2	x	x	x°	—	—
		G3	x	x	x	x	—
		G4	x*	x	x*	x*	x#

Table 2 Maximum values of dimensional accelerations and excursions

	A_G	0.03 *g*			0.04 *g*			0.05 *g*			0.07 *g*		
		v_R	A_{max} (m/s²)	D_{max} (cm)	v_R	A_{max} (m/s²)	D_{max} (cm)	v_R	A_{max} (m/s²)	D_{max} (cm)	v_R	A_{max} (m/s²)	D_{max} (cm)
B0		1.30	1.23	2.95	1.10	1.57	4.60	1.08	2.02	6.73			
B1	G1	1.60	1.73	2.30	1.70	2.39	3.07	1.72	2.81	3.74			
	G2	1.40	1.58	2.59	1.50	2.20	3.17	1.60	2.94	4.18			
	G3	1.30	1.46	2.86	1.50	2.35	3.66	1.60	3.05	4.57			
	G4	1.30	1.23	2.83	1.40	2.34	3.82	1.50	3.12	4.74			
B2	G1	2.00	2.90	1.84	2.30	4.01	2.07	2.50	4.93	2.33			
	G2	1.40	2.52	2.38	1.90	3.77	2.61	2.20	5.16	2.98			
	G3	1.30	1.86	2.67	1.80	4.07	3.14	2.00	5.18	3.32			
	G4	1.20	1.26	3.10	1.55	3.53	3.65	1.75	4.84	3.90			
B3	G1	1.90	2.86	1.84	2.30	4.36	2.01	2.60	4.74	2.28			
	G2	1.50	2.22	2.40	1.90	4.43	2.72	2.15	5.70	2.86			
	G3	1.30	1.99	2.74	1.35	1.72	2.77	1.40	2.19	2.79			
	G4	1.30	1.12	2.67	1.40	2.86	3.30	1.30	6.48	3.82			
B4	G1	2.10	4.34	1.58	2.70	6.51	1.69	3.00	8.03	1.77			
	G2	1.60	3.07	1.99	2.05	5.85	2.05	2.70	9.00	2.22			
	G3	1.60	4.36	2.60	2.10	7.38	2.70	2.40	9.29	2.81	3.00	12.75	2.97
	G4	1.30	1.37	2.88	1.80	6.73	3.20	2.10	9.43	3.28	2.70	13.60	3.50

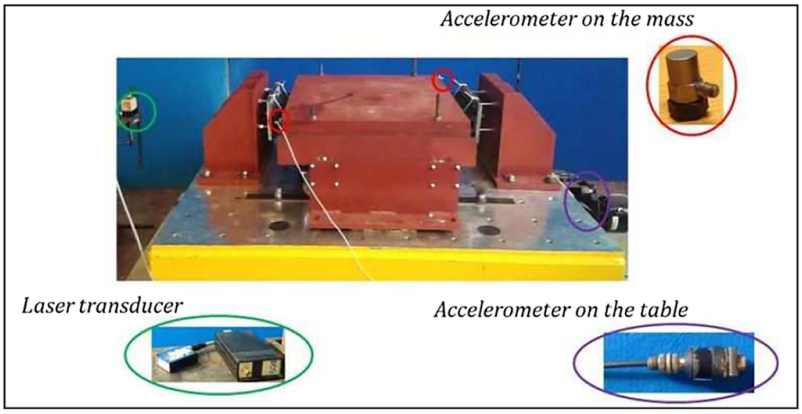

Figure 1 Experimental setup for impact testing

The above-mentioned campaign concerns the nonlinear nonsmooth impact dynamics of a base-isolated (Figure 2a) SDOF oscillator (Figure 1), excited by a harmonic acceleration applied to the base and constrained by two-sided shock absorbers (Figure 2b). The series of experimental investigations considers two distinct configurations: (a) the absence of bumpers (NB) and (b) the presence of bumpers (YB).

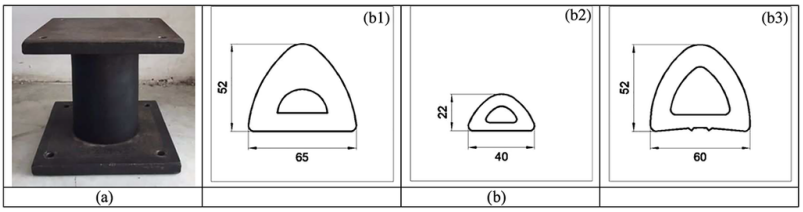

Figure 2 Dissipation devices. (a) Damper and (b) bumpers: (b1) AP 65 × 52, (b2) MB 40 × 22, and (b3) MB 60 × 52

The influence of the most important parameters on the system response, namely, gap width, bumpers' stiffness, and intensity of harmonic excitation is analyzed in order to evaluate the reduction (mitigation) of the dynamic response and the undesirable consequences of outer pounding in the case of PBIS effects in terms of (a) control of excessive displacements, denoted *First Problem* (Section 3.1), and (b) control of excessive absolute accelerations, denoted *Second Problem* (Section 3.2).

2 EXPERIMENTAL SETUP AND TEST DESCRIPTION

The physical model of the SDOF with double-side unilateral constraints under consideration is shown in Figure 1; it consists of (a) a rigid body the can be treated as a lumped mass, M = 500 kg (to simulate the isolated object), (b) an elastomeric isolator, the so-called damper (Figure 2a), (c) two kinds of elastomeric bumpers (Figure 2b) symmetrically mounted on steel stands that are bolted onto the base plate. The mass is comprised of six plates of mild steel jointed by through bolts. The damper is centrally connected to the lower layer of the mass, whereas the clearance between each bumper and the mass, the so-called gap, can be varied by adjusting the screws at the fronts of the stands. The mass is supported by four spherical bearings, rotating within unidirectional guides. The whole system is excited by the shaking table.

2.1 Bumpers

The bumpers used in the campaign of experiments are of three types: AP having a width 65 mm and height 52 mm (Figure 2b1), MB <<Query: AUTHOR: Please define AP and MB if these are abbrevaitions.>>having a width 40 mm and height 22 mm (Figure 2b2), and MB having a width 60 mm and height 52 mm (Figure 2b3); as regards the material,[62] the bumper AP is constituted by an ethylene propylene diene monomer having a hardness of 75 Shore A; and the bumpers MB are constituted by a styrene butadiene rubber copolymer having a hardness of 70 Shore A. Four different bumpers, which were actually used in the tests, were obtained from the three types described above: the bumper B4 was obtained from the bumper AP, using a contact length of L = 400 mm; one bumper (B3) was obtained by the second (MB 40 × 22) type of bumper having length L = 400 mm, and two bumpers were obtained by the third (MB 60 × 52) type of bumper: the bumpers B2 of length L = 400 mm and B1 with L = 100 mm. Bumpers B1–B4 are listed in order of increasing stiffness. For ease of representation, the NB configuration is also referred to below as a B0 bumper.

In terms of relative stiffness, the bumpers can be grouped as follows: B0–B1, B2–B3, and B4. The bumper B0 (also called with the acronym NB) can be interpreted as a bumper associated to an infinite gap or, equivalently, to a bumper of stiffness tending to zero, representing the extreme case of absence of bumpers. The bumper B1 can represent soft bumpers (not very rigid), the bumper B4 can be counted among hard bumpers (very rigid, to the limit comparable with the impact against a rigid obstacle), and bumpers B2 and B3 can be considered representative of a class of bumpers characterized by intermediate stiffness between those of the two previously defined groups.

2.2 Gaps

Four values of the total gap amplitude (i.e., the sum of the single gaps on both sides of the mass), specifically G1 = 15 mm, G2 = 20 mm, G3 = 25 mm, and G4 = 30 mm, were also considered.

2.3 Input signals

The experiments were performed using a vibrating table Moog 1.50 × 1.50 m, managed by Moog Replication Software. Forward and backward sine sweep signals in displacement control were modeled to impose given peak accelerations A_G to the table, along the total frequency ranges f = 0.5–5.0–0.5 Hz. These signals were generated with frequencies f variable in steps, applied for a time sufficient to reach the response's steady state, consisting of 10 cycles within each subfrequency range having a step-size Δf = 0.1 Hz. The input displacement amplitude step-wise decreases as the frequency step-wise increases in the forward sweep (0.5–5.0 Hz) and increases as the frequency step-wise decreases in the backward sweep (5.0–0.5 Hz), Figure 9. In both configurations NB and YB, tests were performed with the same type of exciting action.

2.4 Table accelerations

Four peak values of table acceleration, specifically A_G = 0.03, 0.04, 0.05, 0.07 g (= gravity's acceleration), were imposed.

2.5 Measured response

The measured parameters are the absolute acceleration A of the mass and the relative displacement D of the mass with respect to the vibrating table. Time histories of acceleration and displacement of the table and of the mass were acquired under sinusoidal action applied according to a forward and backward sine sweep, as described above. The acceleration of the mass was measured by the two accelerometers positioned on the mass, in two opposite edges, as shown in Figure 1, and the value A averaged on the two accelerometers has been taken into account. Maximum absolute acceleration values A_{max} were extracted that were recorded at steady state in each subfrequency range of the forward and backward sine sweep. Maximum excursion values E_{max} = (D_{max}

– D_{min}) were recorded at steady state in each subfrequency range of the forward and backward sine sweep; (D_{max} – D_{min}) is the difference between the maximum positive displacement D_{max} and the negative minimum displacement D_{min}. The largest values of acceleration and excursion were attained in the forward sweep, at the so-called pseudoresonance frequency. The displacement of the mass was measured by the laser transducer, as shown in Figure 1. Data acquisition and filtering was performed by means of the KRYPTONw-3xSTG and KRYPTON-4xACC systems by Dewesoft company. The experimental data were acquired with a sampling rate of 2,048 Hz and a second-order Butterworth band pass filter was applied with limiting frequencies of 30.00 and 0.16 Hz.

The series of experimental investigations has considered two distinct configurations: (a) NB and (b) YB.

In the experimental test campaign, the tests carried out deal with several combinations between different situations in terms of absence–presence of the bumpers, type of bumpers, peak acceleration of the table, and amplitude of the gap; therefore, the investigated cases lend themselves to a sufficiently in-depth discussion of the scenarios highlighted in the forced dynamic response of the system. For reader's convenience, Table 1 reports the summary of the tested cases, denoted by "x," where $a_G = A_G/g$. The symbol (*) denotes the common cases between this paper and Andreaus et al.[60, 61]; the symbol (#) denotes the case taken into consideration only in Andreaus et al.[60, 61]; the symbol (o) denotes the cases common to this paper and Andreaus et al.[61]; and the symbol (+) denotes the case studied only in Andreaus et al.[61]

The case A_G = 0.07 g was presented only in cases G3 and G4 because for smaller gaps were observed on one hand a pinball effect consisting in the fact that the mass has a oscillation number greater than that of the table even in opposition phase that generated such high contact forces to influence the input of the table, so as to obtain a table acceleration that was inconsistent with the input we wanted to impose. In support of this, the simulation results in Komodromos et al.[11] indicate that the response may be significantly increased in case of a moat wall on both sides of the building. This behavior is usually more pronounced when the seismic gap is very narrow, in which case it seems that there is a risk of the building bouncing between the two moat walls in a kind of resonance with the earthquake excitation.

3 EXPERIMENTAL RESULTS AND DISCUSSION

With regard to the meaning of the symbols, the colors and the style of the lines, and indicators used in the following figures, the reader is referred to Appendix. In the following, the symbol $a_G = A_G/g$ denotes the nondimensional acceleration amplitude of the shaking table. The exciting action frequency is normalized with respect to the pseudoresonance value relative to the configuration in the absence of bumpers for a_G = 0.1, that is, $f_R \cong$ 1.0 Hz; this case corresponds to a deformation of the damper equal to about 100%; the normalized frequency is indicated by the symbol ν. Both acceleration and excursion are normalized and indicated by the symbols α and η, respectively. Table 2 numerically reports in dimensional form the experimental results that will be graphically shown—in dimensionless form—in Figures 3–8 presented and discussed in the following Sections 3.1 and 3.2.

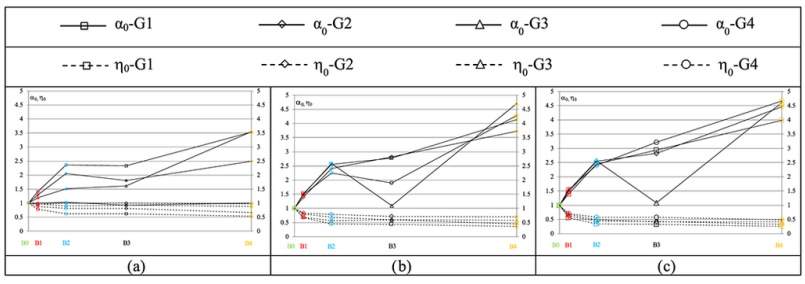

Figure 3 Response in terms of increasing Bumpers' stiffness (acceleration, solid lines; excursion, dashed lines). (a) a_G = 0.03, (b) a_G = 0.04, and (c) a_G = 0.05

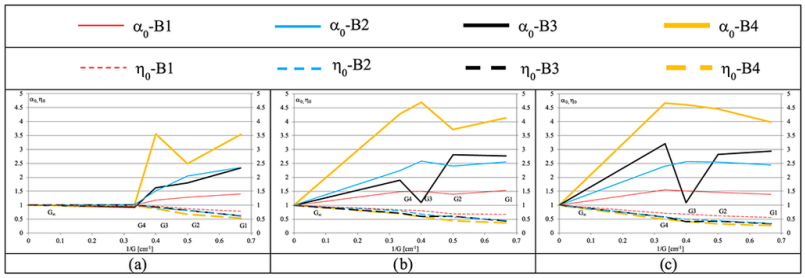

Figure 4 Response in terms of total gap's inverse (acceleration, solid lines; excursion, dashed lines). (a) a_G = 0.03, (b) a_G = 0.04, and (c) a_G = 0.05

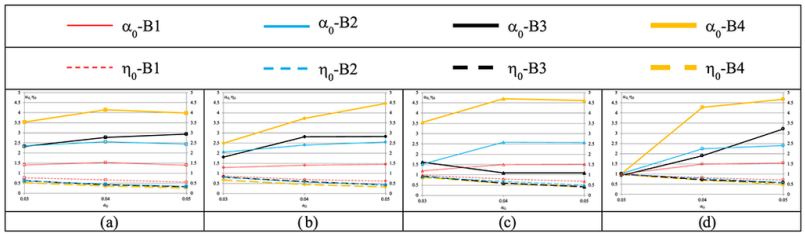

Figure 5 Response in terms of table's acceleration (acceleration, solid lines; excursion, dashed lines). (a) G1, (b) G2, (c) G3, and (d) G4

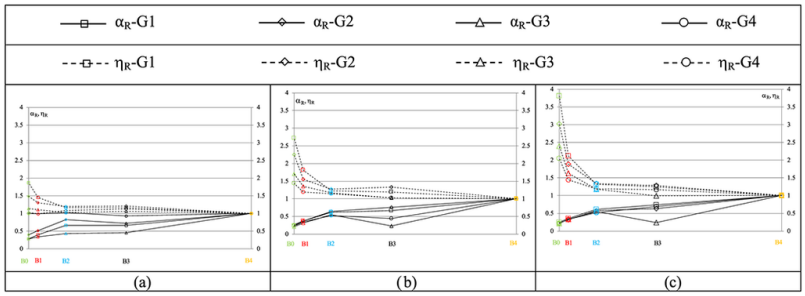

Figure 6 Response in terms of bumpers' stiffness: Acceleration (solid lines) and excursion (dashed lines). (a) a_G = 0.03, (b) a_G = 0.04, and (c) a_G = 0.05

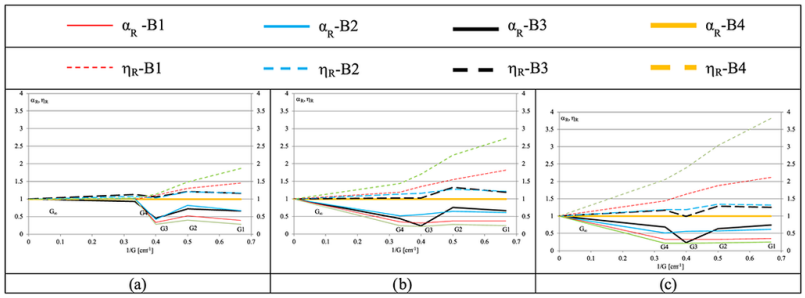

Figure 7 Response in terms of total gap's inverse (acceleration, solid lines; excursion, dashed lines). (a) a_G = 0.03, (b) a_G = 0.04, and (c) a_G = 0.05

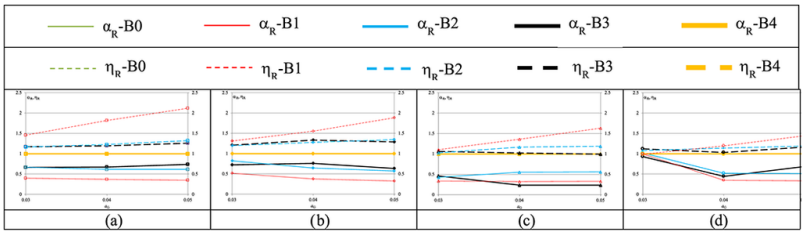

Figure 8 Response in terms of table's acceleration (acceleration, solid lines; excursion, dashed lines). (a) G1, (b) G2, (c) G3, and (d) G4

In the present work, two problems have been identified and studied, with reference to the type of elaboration of the results provided by the experiments and to the aims that with such elaboration arise.

•The First Problem (see Section 3.1) concerns the control of excessive displacements; on the other hand, if the displacements are limited by placing an obstacle, accelerations because of the impact increase. The comparison is made with respect to the situation of absence of obstacle (free flight, NB, or bumper B0). Therefore, normalization is made with respect to the excursion (η_0) and to the acceleration (α_0) in the absence of an obstacle. In the analysis of the response, we consider first η_0 and then α_0, in the sense of fixing (or limiting) admissible values of the excursion (to avoid—for example—possible damage to the damper) while limiting the maximum acceleration values below pre-established thresholds (see Section 3.1 below).

•The Second Problem (see Section 3.2) relates to the control of excessive accelerations that occur when the displacements are to be limited by inserting a rigid obstacle or—as in reality—a bumper with very high relative stiffness; with the insertion of more deformable bumpers, it is possible to limit the accelerations, but one pays the price of an increase in displacement. The normalization is therefore made with respect to the acceleration (α_R) and the excursion (η_R) that occur in the presence of a relatively rigid obstacle (bumper B4). Attention is first paid to the parameter α_R and then to η_R, in the sense of fixing (or limiting) admissible values of acceleration (which could cause possible damage to structural and nonstructural elements, to equipment, etc.) containing the maximum values of displacements below appropriate thresholds (see Section 3.2).

The first and second normalizations are primarily intended for application and can be read in a dual manner.

The results presented in the following are organized according to two problems previously outlined and to the consequential normalizations.

3.1 First problem: Control of excessive displacements

This section is devoted to report and comment mass excursions and accelerations in terms of bumpers' stiffness, gap width, and table acceleration, according to the second type of normalization, that is, with respect to maximum values of excursion and acceleration attained in absence of bumpers (NB/B0). In more detail, the ratio between maximum excursions of mass in presence (E_{max}) and in absence (E_{0max}) of bumpers will be denoted with the symbol $\eta_0 = E_{max}/E_{0max}$, and the ratio between maximum accelerations of mass in presence (A_{max}) and in absence (A_{0max}) of bumpers will be denoted with the symbol $\alpha_0 = A_{max}/A_{max0}$. The mass excursion in the presence of a deformable obstacle is less than that in the absence of an obstacle in the interval $\eta_0 < 1$. The acceleration of the mass in the presence of a deformable obstacle is amplified with respect to the absence of an obstacle in the interval $\alpha_0 > 1$. Both excursion η_0 (dashed line) and acceleration α_0 (solid line) are reported in Figures 3–5.

Figure 3 shows the two quantities in terms of bumpers' stiffness for three different values of the table acceleration a_G = 0.03 (a), 0.04 (b), and 0.05 (c). The symbol B0 means no bumpers, whereas the bumper

B4 can be considered to represent a relatively very stiff obstacle. Excursion and acceleration obviously assume unit values for B0 (absence of bumpers).

Figure 4 reports excursion and acceleration in terms of the inverse of the gap, for three different values of the table acceleration a_G = 0.03 (a), 0.04 (b), and 0.05 (c). The value 1/G = 0 represents the absence of bumpers (G_∞ = gap of infinite width), whereas the value 0.07 represents the smallest gap G1. The colors indicate the different bumpers, according to the convention adopted in the Appendix.

Figure 5 shows excursion and acceleration in terms of the three values of the table accelerations a_G = 0.03 (a), 0.04 (b), and 0.05 (c), for the four different values of the gaps. Furthermore, the bumpers stand out, as usual, for the different colors.

3.1.1 Partial conclusions

The range of variations of η_0 and α_0 are approximately $\eta_0 \cong 0.26$ (bumper B4, a_G = 0.05, gap G1)–1.0 (G_∞) and $\alpha_0 \cong 1.0$ (G_∞)–4.7 (bumper B4, a_G = 0.04, gap G3), respectively. The excursion has a maximum value of 1 and a minimum value of about 0.25; the acceleration has a minimum value of 1 and a maximum value of 4.7. In general, it is found that excursion decreases while acceleration increases with the presence of the bumpers compared with free flight.

Examining the system's response in terms of bumpers' stiffness (Figure 3) shows that excursion decreases with increasing stiffness of the bumpers. Acceleration, however, increases with the stiffness of the bumpers, but in some cases (bumper B3), relative minima are obtained, more and more accentuated with the growth of a_G. As a_G increases, excursion decreases and acceleration increases. Moreover, for the bumpers B2 and B3, zones where excursion and acceleration vary little do exist, even if in some cases the acceleration has a relative minimum.

Analyzing the system's response in terms of total gap's inverse 1/G (Figure 4) reveals that as gap clearance decreases, excursions decrease, while acceleration increases with increasing a_G, according to a curve that exhibits a downward concavity in some cases (a_G = 0.05, B1, B2, B4). For the other gaps, it is not possible to observe the same behavior because the grid of gap and acceleration values experimentally investigated is not sufficiently dense and extensive to allow it.

Studying the system's response in terms of table acceleration a_G (Figure 5) indicates that excursion decreases and acceleration increases, as a_G and gap clearance increase. It is therefore understood that some (both ascending and descending) branches of the curves exhibiting a downward concavity are not visible because some combinations of gap widths and table accelerations could not be implemented because of technical reasons; in fact, the performed campaign of experimental investigations was relatively extensive because of the table's performances and to the characteristics of the experimental setup, as illustrated in Section 2.

The excursion η_0 obviously decreases with increasing stiffness of the bumpers; in particular, η_0 attains the largest and smallest values for B1 and B4, respectively, whereas B2 and B3 remain confined in the band between B1 and B4; η_0 grows as the gap width increases. The trend of η_0 is almost linear, starting from values smaller than 1 in a_G = 0.03 and when G increases; it reaches 1 (again for a_G = 0.03) and “rotates” clockwise as G increases in the sense that the slope decreases, that is, η_0 decreases with the growth of a_G. Thus, the higher a_G, the greater the benefit, as G increases. In particular, η_0 is almost independent of a_G, and there is a constant benefit with respect to a_G for G1.

In a dual way with respect to excursion, acceleration obviously increases as the bumpers' stiffness increases (α_0 attains minimum and maximum values for B1and B4, respectively); bumpers B1 and B2 remain confined in the band between B1and B4 and intersect at different points depending on G. As for the excursion, α_0 translates from top to bottom (up to the value 1 for G4), and “rotates” counterclockwise, in a_G = 0.03 and as G increases.

The bumper B1 appears to be optimal from the point of view of both η_0 and of α_0, for gap clearances that tend to be small, because η_0 is comprised within the range 0.5–1.0, whereas α_0 remains below 1.5 for any G and a_G. Ultimately, the maximum benefit is achieved when B is soft (bumper B1), G is small (gap G1), and a_G is large (a_G = 0.05). We emphasize the importance of the fact that it is more rewarding to obtain larger benefits for large accelerations than for small ones. In fact, the combination of bumper B1 with gap G1 permits to achieve a good compromise between acceleration increase and excursion reduction. This conjuncture corresponds to an optimal situation in the presence of conflicting objectives when the primary objective of controlling the excursions comes into conflict with the unwanted collateral effect of an increase in acceleration.

3.2 Second problem: Control of excessive accelerations

The normalization of the accelerations A_{max} and excursions E_{max} for the various bumpers is now carried out with respect to the corresponding accelerations A_{Rmax} and excursions E_{Rmax} of the stiffest bumper (B4) that, as an approximation, can be assumed to represent the rigid obstacle and leads to the definition of the respective parameters $\alpha_R = A_{max}/A_{Rmax}$ and $\eta_R = E_{max}/E_{Rmax}$. The problem that arises is the excessive acceleration that occurs during the impact with a very (in the limit, infinitely) rigid obstacle. The insertion of deformable bumpers (less rigid than the reference one) allows to limit the accelerations (source of possible damage to structural and nonstructural elements, to equipment, etc.) to the price of accepting a modest increase in the excursions. Thus, attention is first paid to the parameter α_R and then to η_R. The values of α_R and η_R are reported in the ordinates of the Figures 6–8, which are presented and discussed below in analogy with Figures 3–5 of Section 3.1.

The unit value of α_R indicates that the acceleration is equal to that obtained with the rigid obstacle, whereas a unit value of η_R indicates that the excursion is equal to that of the case of the rigid obstacle. With this normalization, it is observed that the accelerations are always between 0 and 1, whereas the excursions are always larger than one. The acceleration of the mass in the presence of a deformable obstacle is reduced with respect to the presence of a rigid obstacle in the interval $\alpha_R < 1$. The mass excursion in the presence of a deformable obstacle is larger than that in the presence of a rigid obstacle in the interval $\eta_R > 1$. This means that for the accelerations, there is always an improvement, whereas for the excursions, there is always a deterioration.

The abscissa axis of Figure 6 shows the various bumpers ordered in the direction of increasing stiffness, and figure parts a, b, and c refer to the three values of a_G = 0.03 (a), 0.04 (b), and 0.05 (c), respectively. Bumper B4 represents the rigid obstacle.

The abscissas of Figure 7a–c show the inverse of the gap width (1/G), and figure parts a, b, and c refer to the three values of a_G = 0.03, 0.04, and 0.05. Read Figure 7a–c from right to left, that is, in the direction of the decreasing abscissae and therefore of the increasing gap.

The table acceleration a_G is given in the abscissas of Figure 8a–d, and figure parts a, b, c, and d refer to the four gap values G1–G4.

3.2.1 Partial conclusions

The above observations made on Figures 6–8 can be synthetized as follows. It is observed (Figures 6–8) that both α_R and η_R have an S-shape in a counterphase (in some cases, there are maxima and minima; in others, only concavity changes); more precisely, a minimum (upward concavity) and a maximum (downward concavity) of η_R correspond to a maximum (downward concavity) and a minimum (upward concavity) of α_R, at varying stiffness and for a given gap.

In absence of bumpers, acceleration (for all gaps) is included in the intervals α_R = 0.28–1.0, 0.21–0.26, and 0.25–0.21 and the excursion in the intervals η_R = 1.9–1.0, 2.7–1.44, and 3.8–2.0, for a_G = 0.03, 0.04, and 0.05,

respectively. The unit value of α_R and η_R for G4 (the largest gap) and a_G = 0.03 (the lowest acceleration of the table) signals the phenomenon of grazing. In presence of bumpers, if we look first of all at the acceleration as a function of the stiffness of the bumpers (Figure 6), we notice a minimum at the bumper B3 and the gap G3, in all the table accelerations but more accentuated with the growth of a_G. Then, going to consider also the excursion in a second moment, we realize that we can make the same observation (made above for acceleration) also for η_R, even if the minimum is less conspicuous, given the flattening of the curves.

Let us now look at the problem in terms of α_R and η_R as a function of G (Figure 7) for the three values of a_G = 0.03, 0.04, and 0.05. For a_G = 0.03, the minimum of α_R for G3 of both B1 (0.33) and B2 (0.43) and B3 (0.46) stands out, whereas η_R = 1.1, 1.03, and 1.06 for B1–B3. For a_G = 0.04, the minimum of α_R = 0.32, 0.55, and 0.23 stands out for B1–B3 at G3, whereas η_R = 1.36, 1.16, and 1.02 for B1–B3. For a_G = 0.05, α_R = 0.33, 0.56, and 0.24 for B1–B3, whereas η_R = 1.63, 1.18, and 1.0 for B1–B3.

From the reading of α_R and η_R in terms of a_G for the various gaps G1–G4 (Figure 8), it is clear that at the gap G3, α_R remains around 0.4 (0.38–0.46) for all the table accelerations, whereas η_R of bumper B3 in G3 is practically equal to 1 (1.0–1.06), coinciding approximately with the excursion limited by the stiffest bumper (B4).

From the comparison of the bumpers B1–B3 at gap G3, we see that the pair B3/G3, compared with the other two pairs B1/G3 and B2/G3, provides a substantial and constant reduction at high (most important) accelerations for both α_R and η_R, showing that the mitigation is stronger in terms of η_R.

The combination between bumper B3 and gap G3 is particularly convenient for all the accelerations examined, as it shows a significant acceleration reduction (0.4–0.5) compared with a modest increase in the excursion (1–1.1), attaining a relative minimum of both α_R and η_R independently of the table acceleration

Thus, it can be stated with reasonable accuracy that from the experimental point of view, there is a particularly significant configuration identified by the pair constituted by the bumper B3 and the gap G3 from the point of view of a significant reduction in accelerations accompanied by a negligible increase in the excursions with respect to the reference response, provided in the case of a rigid obstacle, for all the values of the acceleration of the table that were investigated.

4 COMPARISON BETWEEN EXPERIMENTAL AND NUMERICAL RESULTS

When the mass M is oscillating, three situations exist, and they can be described as follows:

1. The mass is not in contact with any of the bumpers:

$$\begin{cases} M\ddot{D}_d + C_d\dot{D}_d + R_d = -MA_G sin(\Omega t) \\ C_{bj}\dot{D}_{bj} + K_{bj}D_{bj} = 0 \end{cases} \quad (1a)$$

with $G_j(t) > 0$, j = R, L; and

$G_j(t) = G_{oj}(t) + \Delta D_j(t)$

$\Delta D_R(t) = D_{bR}(t) - D_d(t)$

$\Delta D_L(t) = D_d(t) - D_{bL}(t)$;

5 THE MASS IS IN CONTACT WITH THE RIGHT BUMPER (R):

$$\begin{cases} M\ddot{D}_d + C_d\dot{D}_d + R_d + C_{bR}\dot{D}_{bR} + K_{bR}D_{bR} = -MA_G sin(\Omega t) \\ C_{bL}\dot{D}_{bL} + K_{bL}D_{bL} = 0 \end{cases} \quad (1b)$$

with $G_R(t) = 0$ and $D_{bR} = D_d - G_{oR}$;

6 THE MASS IS IN CONTACT WITH THE LEFT BUMPER (L):

$$\begin{cases} M\ddot{D}_d + C_d\dot{D}_d + R_d + C_{bL}\dot{D}_{bL} + K_{bL}D_{bL} = -MA_G sin(\Omega t) \\ C_{bR}\dot{D}_{bR} + K_{bR}D_{bR} = 0 \end{cases} \quad (1c)$$

with $G_L(t) = 0$ and $D_{bL} = D_d - G_{oL}$.

In Equation,[1] D_d is the relative displacement of the damper; D_{bR} and D_{bL} are the relative displacements of right and left bumpers, respectively; K_{bj} and C_{bj} are, respectively, elastic stiffness and damping coefficient of bumpers j = R, L; G_j are the gap functions of bumpers j = R, L; G_{oj} are the initial gaps of bumpers j = R, L; and A_G and Ω are peak and frequency of the acceleration input applied by the table.

The definition of R_d appearing in Equation[1] above will be given in Equation[2] below.

The piecewise-linear restoring force of the damper obeys the following constitutive law in the ($D_d \geq 0$, $R_d \geq 0$) region:

$$R_d = K_{d1}D_d \quad 0 \leq R_d \leq R_{d1} \text{ 1st elastic branch} \quad (2a)$$

$$R_d = R_{d1} + K_{d2}(D_d - D_{d1}) \quad R_{d1} \leq R_d \leq R_{d2} \text{ 2nd elastic branch} \quad (2b)$$

$$R_d = R_{d2} + K_{d3}(D_d - D_{d2}) \quad R_{d2} \leq R_d \text{ 3rd elastic branch,} \quad (3c)$$

where D_d and R_d are the current values of displacement and force; D_{d1} and D_{d2} are the displacements corresponding to forces R_{d1} and R_{d2}. Analogous laws hold in the ($D_d \leq 0$, $R_d \leq 0$)-region. Each bumper is massless and exerts on the mass (in the contact phase) a linearly elastic restoring force characterized by elastic stiffness K_{bj} (j = R, L).

The values of mechanical parameters characterizing the constitutive laws of damper and bumpers B1 and B2 that have been identified and then adopted in the numerical model to simulate sample experimental results by using a general-purpose computer code (Sap2000 v.20) are reported in this section; the identification of the above-mentioned bumpers had not been presented in Andreaus et al.[60, 61] In this paper, the experimental and numerical responses of the system was analyzed and compared in the configuration characterized by low-middle stiffness bumpers B1 and B2 and the low-middle gap G2, under a step-wise forward and backward sine sweep (ranges f = 0.5–5.0–0.5 Hz and step-size Δf = 0.1 Hz), characterized by constant A_G = 0.05 g, performing a sufficient number of cycles to reach the steady state. The piece-wise tri-linear elastic behavior of the damper was modeled with stiffness K_{d1} = 20 kN/m between displacements D_{d1} = 0 and D_{d2} = 8 mm, and forces R_{d1} = 0 and R_{d2} = 0.160 kN, K_{d2} = 18 kN/m between displacements D_{d2} = 8 and D_{d3} = 40 mm, and forces R_{d2} = 0.160 and R_{d3} = 0.736 kN, K_{d3} = 2 kN/m for $D_d > D_{d3}$ = 40 mm and $R_d > R_{d3}$ = 0.736 kN; analogous laws hold in the ($D_d \leq 0$, $R_d \leq 0$) region. The linear viscous behavior of damper was identified by the damping coefficient C_d = 1.1 kNs/m. The linear elastic behavior of the bumpers was modeled with a stiffness K_{B1} = 33 kN/m for bumper B1 and K_{B2} = 175 kN/m for bumper B2; the linear viscous behavior of the bumpers

was identified by the damping coefficients C_{B1} = 0.3 kNs/m and C_{B2} = 0.5 kNs/m, for the bumpers B1 and B2, respectively.

The proposed numerical model has been implemented in the SAP2000 v.20 proprietary code; the system was subject to a table input consisting in a step-wise displacement, which is characterized by the forward and backward sine sweep shown in Figure 9, along the frequency ranges f = 0.5–5.0 Hz in forward sweep and f = 5.0–0.5 Hz in backward sweep, with step-size Δf = 0.1 Hz and which corresponds to a constant acceleration peak A_G = 0.05 g.

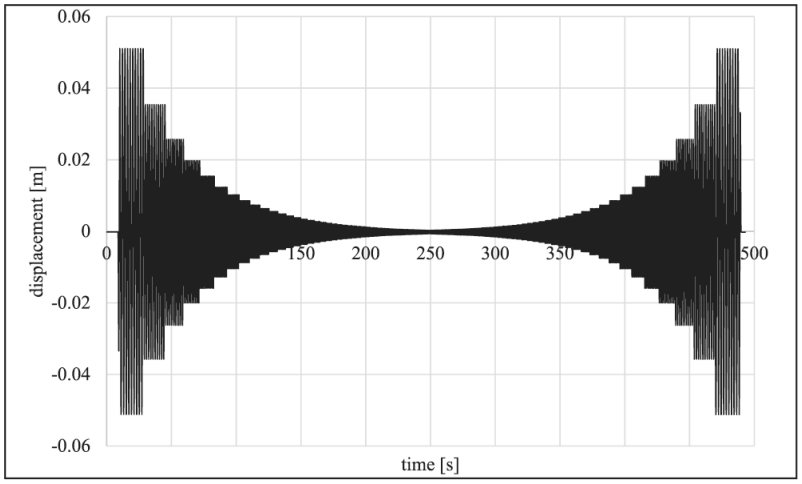

Figure 9 Forward and backward sine sweep of table input displacement (f = 0.5–5.0–0.5 Hz, A_G = 0.05 g, Δf = 0.1 Hz)

Two cases were examined, namely, bumpers B1 and B2 with gap G2 and table acceleration A3, and the numerical results were compared with the experimental ones in terms of (a) displacement and acceleration time histories along the total time ranges, (b) pseudoresonance curves along the frequency ranges f = 0.5–5.0 Hz in forward sweep and f = 5.0–0.5 Hz in backward sweep, and (c) hysteresis loops and phase portraits at pseudoresonance, which is understood as the frequency where the maximum response is attained, that is, the largest amplitude oscillation is exhibited in the forward portion of the applied sine sweep; the hysteresis loops plot absolute acceleration in terms of relative displacement of the mass; the absolute acceleration is related to the inertia force and hence to the total force acting on the mass.

In particular, Figures 10 and 11 (bumper B1) show forward and backward time histories of experimental (Figure 10) and numerical (Figure 11) responses for (a) absolute acceleration and (b) excursion of relative displacement. Figure 12 (bumper B1) shows the forward and backward pseudoresonance curves for (a) absolute value of absolute acceleration and (b) excursion of relative displacement. Figures 13 (bumper B1) and 14 (bumper B2) show hysteresis loops (a) and phase portraits (b) at resonance.

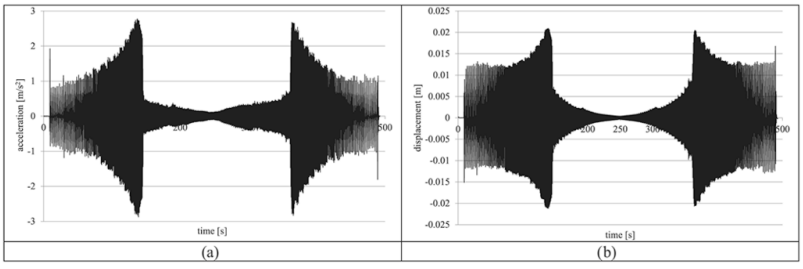

Figure 10 Forward and backward time-histories of experimental responses (bumper B1). (a) Absolute acceleration and (b) relative displacement

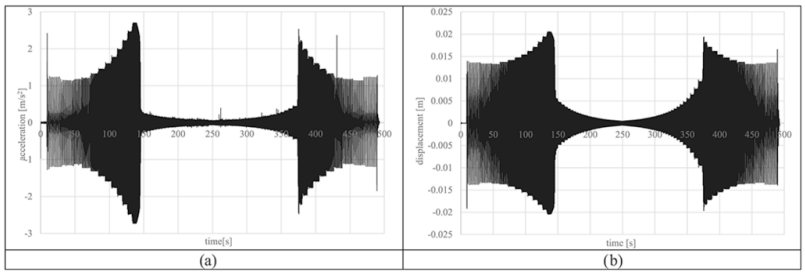

Figure 11 Forward and backward time-histories of numerical responses (bumper B1). (a) Absolute acceleration and (b) relative displacement

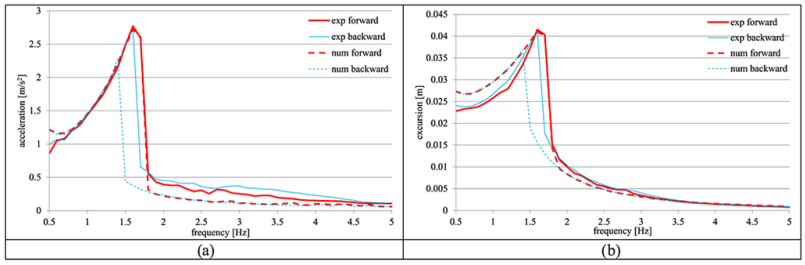

Figure 12 Pseudoresonance curves (bumper B1). (a) Acceleration and (b) excursion

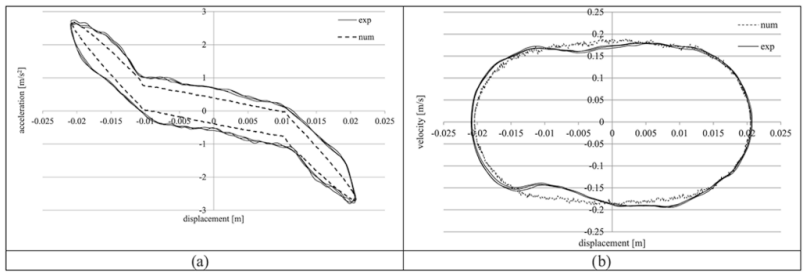

Figure 13 Experimental and numerical maximum responses (bumper B1). (a) Hysteresis loops and (b) phase portraits

A suitable model has been developed to numerically simulate the behavior of the system by using a general-purpose computer code, achieving a good agreement with the experimental results.

As far as the case B1 is concerned, comparing pseudoresonance curves (Figure 12), hysteresis loops of absolute acceleration versus relative displacement at resonance (Figure 13a) and phase portraits (relative velocity vs. relative displacement) at resonance (Figure 13b) shows a good agreement between numerical and experimental results.

In Figure 12, experimental and numerical results are indicated by solid and dashed lines respectively, whereas forward (red color) and backward (blue color) sweeps are denoted by thick and thin lines, respectively.

In Figure 13, experimental and numerical results are indicated by solid and dashed lines, respectively.

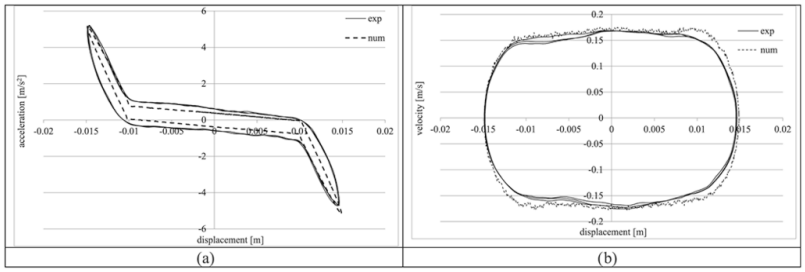

Figure 14 Experimental and numerical maximum responses (bumper B2). (a) Hysteresis loops and (b) phase portraits

As far as the case B2 is concerned, comparing hysteresis loops of absolute acceleration versus relative displacement at resonance (Figure 14a) and phase portraits (relative velocity vs. relative displacement) at resonance (Figure 14b) shows a good agreement between numerical and experimental results.

7 CONCLUSIONS

In this paper, an experimental investigation is presented about two-sided damping constraint technique for end-stop impact protection, when the system is subjected to base harmonic excitation. The physical model of the SDOF system with double-side unilateral constraints under consideration consists of a rigid body that can be treated as a lumped mass, an elastomeric isolator (the so-called damper), and some kinds of elastomeric shock absorbers (the so-called bumpers), mounted symmetrically on steel stands that are bolted onto the base plate. The damper is centrally located with respect to the mass, whereas the clearance between bumpers and mass, the so-called gap, was varied within a suitable range.

A first result obtained in the present work was that of having given a bibliographic framework of the recent scientific literature on the subject of structural pounding of isolated structures at the base, on the basis of some key words, such as pounding between adjacent structures, pounding of the structure against moat walls at the base, pounding between adjacent structures and with moat walls, numerical and/or experimental approach, one or more degrees of freedom, 2-D/3-D, sinusoidal action and/or seismic action, theoretical and/or applicative papers, and linear or nonlinear behavior of isolators.

The experimental tests on the vibrating table have considered two different configurations: the absence of bumpers and the presence of bumpers. Four different values of the table acceleration peak were applied, four different amplitude values of the total gap between mass and bumpers were considered, and finally, also four different types of bumpers were employed. The performed tests are summarized in Table 2; they contemplate several combinations among the different situations in terms of the absence–presence of the bumpers, type of bumpers, gap clearance, and acceleration peak of the table. The campaign of experimental investigations carried out in the present work is relatively extensive, limited to the table's performances and to the characteristics of the experimental setup. From the information given in Table 1, it can be deduced that the cases studied in the present work are about five times those studied in the previous articles.[60, 61]

The processing of the system's response was conducted by addressing two fundamental problems illustrated in Sections 3.1 and 3.2, respectively.

Section 3.1 concerns the control of excessive displacements; on the other hand, if the displacements are limited by placing an obstacle, accelerations because of the impact increase. The comparison is made with respect to the situation of absence of obstacle, that is, free flight. The indication can be given that a soft bumper (B1) and a small gap (G1) are a good compromise between acceleration increase and excursion reduction for this problem, within the limitations of the performed experimental tests.

Section 3.2 relates to the control of excessive accelerations that occur when the displacements are to be limited by inserting a rigid obstacle or—as in reality—a bumper with very high relative stiffness, that is, the stiffest bumper B4; with the insertion of more deformable bumpers, it is possible to limit the accelerations, but one pays the price of an increase in displacement. Intermediate bumpers' stiffnesses (e.g., bumper B3) and gap widths (e.g., gap G3) could be a satisfactory choice for this second problem.

Definitively, as for experimental investigation, the results obtained in the two examined problems suggest an acceptable trade-off between conflicting objectives.

Finally, a suitable numerical model based on a trilinear elastic and linearly viscous isolator and on linear viscous-elastic bumpers has been proposed and implemented in a general-purpose calculation code, identifying the values of the constitutive parameters on the basis of the available experimental results. The comparison between the numerical results thus obtained, and the experimental results had a satisfactory outcome also relatively to the two new bumpers examined in this paper.

ACKNOWLEDGMENTS

This research was funded by the Italian Ministry of University and Research, under the Scientific Research Program of Relevant National Interest: Year 2010–2011, Protocol 2010MBJK5B-005, Title “Dynamics, Stability and Control of Flexible Structures.”

REFERENCES

[1] Kelly JM. *Earthquake-Resistant Design with Rubber*. London: Springer; 1997.

[2] Ismail M, Rodellar J, Pozo F. Passive and hybrid mitigation of potential near-fault inner pounding of a self-braking seismic isolator. *Soil Dyn Earthq Eng*. 2015; **69**:233-250.

[3] Jangid R, Kelly J. Base isolation for near-fault motions. *Earthq Eng Struct Dyn*. 2001; **30**:691-707.

[4] Murat D, Srikanth B. Equivalent linear analysis of seismic-isolated bridges subjected to near-fault ground motions with forward rupture directivity effect. *Eng Struct*. 2007; **29**:21-32.

[5] Reggio A, De Angelis M. Optimal energy-based seismic design of non-conventional tuned mass damper (TMD) implemented via inter-story isolation. *Earthq Eng Struct Dyn*. 2015; **44**(10):1623-1642.

[6] Reggio A, De Angelis M. Optimal design of an equipment isolation system with nonlinear hysteretic behaviour. *Earthq Engng Struct Dyn*. 2013; **42**(13):1907-1930.

[7] Lu L-Y, Lee T-Y, Juang S-Y, Yeh S-W. Polynomial friction pendulum isolators (PFPIs) for building floor isolation: an experimental and theoretical study. *Eng Struct*. 2013; **56**:970-982.

[8] Reggio A, De Angelis M. Combined primary-secondary system approach to the design of an equipment isolation system with high-damping rubber bearings. *J Sound Vib*. 2014; **333**(9):2386-2403.

[9] <<Query: AUTHOR: "First Page, Last Page" elements are required. Please provide.>>Polycarpou PC, Komodromos P. On poundings of a seismically isolated building with adjacent structures during strong earthquakes. *Earthq Engng Struct Dyn* 2010a; 39(8): 933–940. *Short Communication*.

[10] Mavronicola EA, Polycarpou PC, Komodromos P. Effect of planar impact modeling on the pounding response of base-isolated buildings. *Front Built Environ*. 2016; **2**(11):1-16.

[11] Komodromos P, Polycarpou PC, Papaloizou L, Phocas MC. Response of seismically isolated buildings considering poundings. *Earthq Engng Struct Dyn*. 2007; **36**(12):1605-1622.

[12] Anagnostopoulos SA. Pounding of buildings in series during earthquakes. *Earthq Engng Struct Dyn*. 1988; **16**(3):443-456.

[13] Papadrakakis M, Mouzakis H. Earthquake simulator testing of pounding between adjacent buildings. *Earthq Engng Struct Dyn*. 1995; **24**(6):811-834.

[14] Masroor A, Mosqueda G. Experimental simulation of base-isolated buildings pounding against moat wall and effects on superstructure response. *Earthq Engng Struct Dyn*. 2012; **41**(14):2093-2109.

[15] Polycarpou PC, Komodromos P, Polycarpou AC. A nonlinear impact model for simulating the use of rubber shock absorbers for mitigating the effects of structural pounding during earthquakes. *Earthq Eng Struct Dyn*. 2013; **42**(1):81-100.

[16] Crozet V, Politopoulos I, Yang M, Martinez J-M, Erlicher S. Sensitivity analysis of pounding between adjacent structures. *Earthq Engng Struct Dyn*. 2018; **47**(1):219-235.

[17] Polycarpou PC, Komodromos P. Numerical investigation of potential mitigation measures for poundings of seismically isolated buildings. *Earthq Struct*. 2011; **2**(1):1-24.

[18] Zhang W, Xu Y. Vibration analysis of two buildings linked by Maxwell model defined fluid dampers. *J Sound Vib*. 2000; **233**(5):775-796.

[19] Zhu H, Xu Y. Optimum parameters of Maxwell model-defined dampers used to link adjacent structures. *J Sound Vib*. 2005; **279**(1–2):253-274.

[20] Bhaskararao A, Jangid R. Harmonic response of adjacent structures connected with a friction damper. *J Sound Vib*. 2006; **292**(3–5):710-725.

[21] Basili M, De Angelis M. Optimal passive control of adjacent structures interconnected with nonlinear hysteretic devices. *J Sound Vib*. 2007a; **301**(1–2):106-125.

[22] Basili M, De Angelis M. A reduced order model for optimal design of 2-mdof adjacent structures connected by hysteretic dampers. *J Sound Vib*. 2007b; **306**(1–2):297-317.

[23] Zhu H, Ge D, Huang X. Optimum connecting dampers to reduce the seismic responses of parallel structures. *J Sound Vib*. 2011; **330**(9):1931-1949.

[24] Agarwal V, Niedzwecki J, van de Lindt J. Earthquake induced pounding in friction varying base isolated buildings. *Eng Struct*. 2007; **29**(11):2825-2832.

[25] Chase JG, Boyer F, Rodgers GW, Labrosse G, Macrae GA. Probabilistic risk analysis of structural impact in seismic events for linear and nonlinear systems. *Earthq Engng Struct Dyn*. 2014; **43**(10):1565-1580.

[26] Wang J, Shen Y, Yang S. Dynamical analysis of a single degree-of-freedom impact oscillator with impulse excitation. *Adv Mech Eng*. 2017a; **9**(7):1-10.

[27] Sołtysik B, Falborski T, Jankowski R. Preventing of earthquake-induced pounding between steel structures by using polymer elements-experimental study. *Procedia Engineer*. 2017; **199**:278-283.

[28] Mate NU, Bakre SV, Jaiswal OR. Seismic pounding response of singled-degree-of-freedom elastic and inelastic structures using passive tuned mass damper. *Int J Civ Eng*. 2017; **15**(7):991-1005.

[29] <<Query: AUTHOR: “First Page, Last Page” elements are required. Please provide.>>Bamer F, Shi J, Markert B. Efficient solution of the multiple seismic pounding problem using hierarchical substructure techniques. *Comput Mech* 2017: 1–22. *Article in Press*.

[30] <<Query: AUTHOR: “First Page, Last Page” elements are required. Please provide.>>Wang W, Hua X, Wang X, Chen Z, Song G. Advanced impact force model for low-speed pounding between viscoelastic materials and steel. *J Eng Mech*. 2017b; **143**(12):04017139.

[31] Malhotra P. Dynamics of seismic impacts in base-isolated buildings. *Earthq Engng Struct Dyn*. 1997; **26**(8):797-813.

[32] Matsagar V, Jangid R. Seismic response of base-isolated structures during impact with adjacent structures. *Eng Struct*. 2003; **25**(10):1311-1323.

[33] <<Query: AUTHOR: “First Page, Last Page” elements are required. Please provide.>>Hao H, Bi KM, Chouw N, Ren WX. State-of-the-art review on seismic induced pounding response of bridge structures. *J of Earthq Tsunami*. 2013; **7**(3):1350019). 1–1350019-19

[34] Guo AX, Li ZJ, Li H, Ou JP. Experimental and analytical study on pounding reduction of base-isolated highway bridges using MR dampers. *Earthq Engng Struct Dyn*. 2009; **38**(11):1307-1333.

[35] Sun H, Li B, Bi K, Chouw N, Butterworth JW, Hao H. Shake table test of a three-span bridge model. Proceedings of the Ninth Pacific Conference on Earthquake Engineering “Building an Earthquake-Resilient Society”, Auckland, New Zealand, 14–16 April 2011, Paper Number 149.

[36] Jankowski R, Wilde K, Fujino Y. Reduction of pounding effects in elevated bridges during earthquakes. *Earthquake Engineering and Structural Dynamics*. 2000; **29**(2):195-212.

[37] Zanardo G, Hao H, Modena C. Seismic response of multi-span simply supported bridges to a spatially varying earthquake ground motion. *Earthq Eng Struct Dyn*. 2002; **31**(6):1325-1345.

[38] Saadeghvaziri MA, Yazdani-Motlagh A. Inelastic seismic response of stiffening systems and development of demand spectrum: application to MSSS bridges. *Earthq Eng Struct Dyn*. 2007; **36**(14):2153-2169.

[39] Bi KM, Hao H, Chouw N. Required separation distance between decks and at abutments of a bridge crossing a canyon site to avoid seismic pounding. *Earthq Eng Struct Dyn*. 2010; **39**(3):303-323.

[40] Li B, Bi KM, Chouw N, Butterworth JW, Hao H. Experimental investigation of spatially varying effect of ground motions on bridge pounding. *Earthq Engng Struct Dyn*. 2012; **41**(14):1959-1976.

[41] Zhu P, Abe M, Fujino Y. Modelling three-dimensional non-linear seismic performance of elevated bridges with emphasis on pounding of girders. *Earthq Eng Struct Dyn*. 2002; **31**(11):1891-1913.

[42] Guo AX, Cui LL, Li H. Impact stiffness of the contact-element models for the pounding analysis of highway bridges: experimental evaluation. *J Earthq Eng*. 2012; **16**(8):1132-1160.

[43] Li-Xiang H, Shrestha B, Hao H, Bi K-M, Ren W-X. Experimental and three-dimensional finite element method studies on pounding responses of bridge structures subjected to spatially varying ground motions. *Adv Struct Eng*. 2017; **20**(1):105-124.

[44] Tsai H. Dynamic analysis of base-isolated shear beams bumping against stops. *Earthq Eng Struct Dyn*. 1997; **26**(5):515-528.

[45] Komodromos P. Simulation of the earthquake-induced pounding of seismically isolated buildings. *Comput Struct*. 2008; **86**(7–8):618-626.

[46] Liu C, Yang W, Yan Z, Lu Z, Luo N. Base pounding model and response analysis of base-isolated structures under earthquake excitation. *Applied Sciences*. 2017, 12; **7**:1-16. Article number 1238

[47] Masroor A, Mosqueda G. Impact model for simulation of base isolated buildings impacting flexible moat walls. *Earthq Eng Struct Dyn*. 2013; **42**(3):357-376.

[48] Polycarpou P, Komodromos P. Earthquake-induced poundings of a seismically isolated building with adjacent structures. *Eng Struct*. 2010b; **32**(7):1937-1951.

[49] Pant DR, Wijeyewickrema AC. Structural performance of a base-isolated reinforced concrete building subjected to seismic pounding. *Earthq Eng Struct Dyn*. 2012; **41**(12):1709-1716.

[50] Harvey PS Jr, Gavin HP. Double rolling isolation systems: a mathematical model and experimental validation. *Int J Nonlin Mech*. 2014; **61**:80-92.

[51] Harvey PS Jr, Zéhil G-P, Gavin HP. Experimental validation of a simplified model for rolling isolation systems. *Earthq Eng Struct Dyn*. 2014; **43**(7):1067-1088.

[52] Harvey PS, Gavin HP. Assessment of a rolling isolation system using reduced order structural models. *Eng Struct*. 2015; **99**:708-725.

[53] Ismail M, Rodellar J, Ikhouane F. An innovative isolation device for aseismic design. *Eng Struct*. 2010; **32**(4):1168-1183.

[54] Ismail M, Rodellar J. Experimental investigations of a rolling-based seismic isolation system. *J Vib Control*. 2018; **24**(2):323-342.

[55] Fenz DM, Constantinou MC. Behaviour of the double concave friction pendulum bearing. *Earthq Eng Struct Dyn*. 2006; **35**(11):1403-1424.

[56] Yue L, Kehai W, Qiqi W. Experiment of ultimate shear failure and friction sliding performance of rubber bearings of bridges. *Open Civ Eng J*. 2017; **11**:586-597.

[57] Wu G, Wang K, Lu G, Zhang P. An experimental investigation of unbonded laminated elastomeric bearings and the seismic evaluations of highway bridges with tested bearing components. *Shock Vib*. 2018Article ID 8439321;1-18.

[58] Tsai CS, Chiang T-C, Chen B-J, Lin S-B. An advanced analytical model for high damping rubber bearings. *Earthq Eng Struct Dyn*. 2003; **32**(9):1373-1387.

[59] Andreaus U, De Angelis M. Nonlinear dynamic response of a base-excited SDOF oscillator with double-side unilateral constraints. *Nonlinear Dynam*. 2016; **84**(3):1447-1467.

[60] <<Query: AUTHOR: "First Page, Last Page" elements are required. Please provide.>>Andreaus U, Baragatti P, De Angelis M, Perno S. A preliminary experimental study about two-sided impacting SDOF oscillator under harmonic excitation. *J Computat Nonlin Dyn*. 2017a; **12**(6):061010. -1-061010-10

[61] Andreaus U, Baragatti P, De Angelis M, Perno S. Shaking table tests and numerical investigation of two-sided damping constraint for end-stop impact protection. *Nonlinear Dynam*. 2017b; **90**(4):2387-2421.

[62] Núñez K, Rivas L, Scattolini M, Rosales C, Perera R, Matos M. Mechanical properties of TPVs of EPDM/polypropylene/paraffin oil. *Rev Téc Ing Univ Zulia*. 2007; **30**:445-453.

APPENDIX A.:

The meaning of the symbols, the colors and the style of the lines and indicators used in the figures of Section 4 is explained in the following *legenda*.

Bumper B (line color, increasing stiffness *K*, *L* length of the bumper [mm])

B1 MB 60 × 52 L100

B2 MB 60 × 52 L400

B3 MB 40 × 22 L400

B4 AP 65 × 52 L400

Gap G (indicator form, increasing amplitude G)

G1 15 mm □

G2 20 mm ◇

G3 25 mm △

G4 30 mm ○

Acceleration a_G (line style)

a_{G1} 0.03 ——

a_{G2} 0.04 - - - - -

a_{G3} 0.05

a_{G4} 0.07

Acceleration a_G (indicator size, increasing amplitude of a_G)

G1 □ □ □ □

G2 ◇ ◇ ◇ ◇

G3 △ △ △ △

G3 ○ ○ ○ ○